ISSN (Print): 0974-6846
ISSN (Online): 0974-5645
Indian Journal of Science and Technology, *Vol 12(31), DOI: 10.17485/ijst/2019/v12i31/146623, August 2019*

A Control Strategies of PV System based on VOC, SMC and MPC Algorithms

H. Laabidi[1,2*], H. Jouini[2] and A. Mami[2]

[1]ESPRIT School of Engineering, Tunis, Tunisia; houda.abidi@esprit.tn
[2]University Tunis El Manar, Laboratory LAPER, Tunis, Tunisia; houda.jouini@gmail.com, abdelkader.mami@fst.rnu.tn

Abstract

Objectives: Due to the stochastic behavior of the climatic conditions, a comparative study of grid- connected PV inverter based on Voltage Oriented Control (VOC), Sliding Mode Control (SMC) and the proposed Model Predictive Control (MPC) method is required to enhance the power quality that is affected by the weather fluctuations, and to ensure unremitting operation at the maximum power point in order to inject to grid the totality of the generated electrical energy. **Methodology:** The PV power extracted from the PV array is fed to grid via a three phase inverter interface by maintaining constant DC-link voltage. To evaluate the MPC algorithm efficiency for controlling this power inverter, it's necessary to compare its performances to already studied techniques. Comparative case studies often introduce qualitative criteria such as waveforms, current Total Harmonic Distortion (THD), power distortion and switching frequency. **Findings:** The simulation results under Psim environment prove the MPC-based algorithm robustness to control the photovoltaic inverter, particularly, the lower overshoots, the accuracy and the minimum current THD. **Improvement:** The obtained Psim simulations validate the effectiveness of the proposed MPC method against parameter variations.

Keywords: Grid, PV System, MPC, VOC, SMC

1. Introduction

Three-phase grid connected inverters are mostly employed for a wide variety of sectors, such as electrical drive systems, loads fed through AC-DC converters and distributed power generations including renewable energy field. Actually, distributed power generation based on photovoltaic energy is considered one of the world's fastest increasing sources, serving to compensate the rising energy demands and reducing the environmental issues. Otherwise, the Photovoltaic (PV) system control techniques have gained increasing attention into the research community during the last two decades due to the high power electronic devices progress, on one hand, the microelectronic expansion as well as the digital control card architectures revolution is in the other hand.

The control scheme of a grid-connected PV system is generally composed of two parts; the first one consist of controlling the DC/DC converter based on MPPT algorithm, although the second part is adopted to control a three phase inverter which is required to connect the PV energy conversion system to the electrical grid. There are many approaches for evaluating PV system's MPPT algorithm presented in literature. Fuzzy Logic (FL) Controller applied for MPPT is investigated by[1] and it is compared to a basic tracking algorithm Perturb and Observe (P&O). The Fuzzy Logic approach presents some problems such as implementation complexity and high cost. In[2], a Maximum Power Point Tracking (MPPT) based on Model Predictive Controller (MPC) technique is compared with P&O and classical Incremental Conductance (IC) algorithms under different level irradiances. Despite

*Author for correspondence

their simplicity, P&O and IC methods show an unavoidable oscillation drawback; however, the MPC algorithm can present a better dynamic. Other studies given by [3–6] showed that the MPC algorithm adopted for MPPT controller is employed to enhance the efficiency of PV energy conversion system. From all these investigations mentioned above, we can retain the INC-MPC method importance for controlling the MPPT to extract the maximum power.

Recently, researches have focused on the three phase grid connected inverter control which is divided into three steps; Firstly, the dc-link voltage regulation using a PI controller is intended to determine the direct current reference. The output grid currents control is depicted in the second step and the Phased Locked Loop (PLL) is basically used to give an estimation of the lattice voltage edge in the last step. The current control loops are considered the major key tasks in the grid connected converter command since it consists in controlling the active and the reactive power injected into the grid. In fact, several current control techniques have been investigated in literature. The conventional linear control methods based on proportional-integral(PI) was presented by[7] showing that the Voltage-Oriented Control (VOC) strategy is applied for the voltage source inverter (VSI) due to its simple structure with a constant frequency switching; other than one of the most amazing disadvantages is their exceptionally reliance on framework parameter varieties. Another study given by[8] has focused on the non-linear hysteresis control of a grid connected PV system, the Direct Power Control (DPC), that is applied in this study, is consisting to select the inverter switching states from a switching table based on the errors between the active and reactive measured powers and their corresponding reference signals, however, the high current harmonic distortion caused by the switching frequency variation is the main problems of this method. Both[9,10] showing two internal current loops controlled by the Sliding Mode Control (SMC) due to its robustness against parameters variation, but, a higher current THD is the major drawbacks of this technique. Actually, the Model Predictive Control (MPC) is the most promising PV inverter techniques[11–14].

The raison for the considerable interest in the MPC application in these areas is the mathematical models use in order to predict the future behavior of the system controlled variables. Nowadays, the existence of robust microprocessors and powerful digital cards allow to perform the large number calculations needed in MPC.

In this context, this study aims to extract a grid connected photovoltaic converter behavior using MPC algorithm under different meteorological conditions. The thought behind MPC is to limit the cost capacity or the blunder between the anticipated qualities and their references, MPC-based calculation license to choose and apply the ideal voltage vector. To evaluate the ability of this proposed method for controlling power converters, a comparison between MPC schemes and conventional techniques like VOC and SMC is carried out using computer simulations.

Thus, this work is structured as follows; the photovoltaic system architecture and its mathematical models are presented in the first section. Then, the Maximum Power Point Tracking (MPPT) control and the grid connected converter control techniques are illustrated. In the third section, a comparative study of performance analysis based on Psim software simulations are carried out to show the validity of the proposed MPC algorithm and to verify its effectiveness.

2. PV System Configuration

The proposed PV grid connected system is described by Figure 1. It is composed of two conversion parts; the first one consists of PV module as energy source connected to DC/DC converter using a boost chopper. The MPPT controller based on IC-MPC algorithmic applied in this study to extract the maximum power. The grid side converter presented in the second part is equipped with its three phase inverter coupled to RL filter to eliminate the current harmonics. The inverter control system seeks to compare the proposed MPC method with VOC and SMC classical methods. The main goals of the employed techniques are to regulate the active and reactive power by controlling of the d and q grid current components and to improve the injected power superiority into the grid. The numerical models of each square are presented in the accompanying subsections.

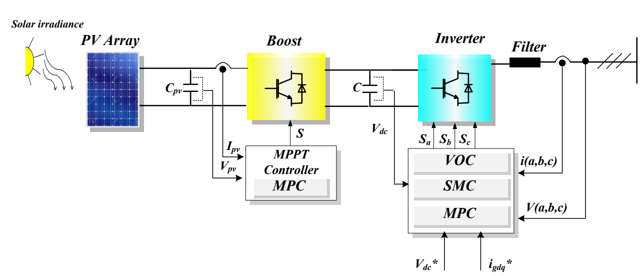

Figure 1. PV power system structure.

3. The Photovoltaic System Modeling

3.1 The Photovoltaic Generator

By methods for the photoelectric wonders, the sun based cell can straightforwardly convert the sunlight to electric power. The photovoltaic comparable circuit is depicted in Figure 2. It is made out of a present source in parallel with a diode, arrangement opposition *(R_S)* and a shunt obstruction *(R_p)*.

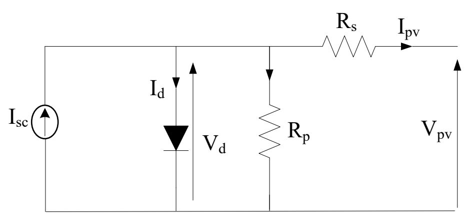

Figure 2. Single photovoltaic cell model.

The mathematical equation for voltage and the current of PV cell is stated as follows:

$$I_{pv} = I_{sc} - I_d - \frac{V_d}{R_p} \tag{1}$$

$$I_d = I_s\left(e^{\frac{V_d}{Vt}} - 1\right) \tag{2}$$

$$V_t = \frac{nKT}{q} \tag{3}$$

$$V_d = V_{PV} + I_{pv} * R_S \tag{4}$$

where, I_{sc} is the short-circuit current due to photons (A), I_d is the diode current, I_s is the diode opposite saturation current (A), n is the joint constant, q is the electron charge (q = 1.6 × 10^{-19} C), k is the Boltzmann continuous (1.3806505 × 10^{-23} J/K), T is the cell temperature (in Kelvin), I_{pv} is the valued current at extreme power point (MPP) (A), V_{PV} is the regarded voltage at extreme power point (MPP) (V).

3.2 MPPT Controller using IC-MPC Algorithm

The Switched DC/DC circuit is commonly used to remove the greatest power from the PV cluster. It has two operation modes; the first switching state, when the switch S is opened (S = 1); and the second one when the switch is closed (S = 0) as shown on Figure 3.

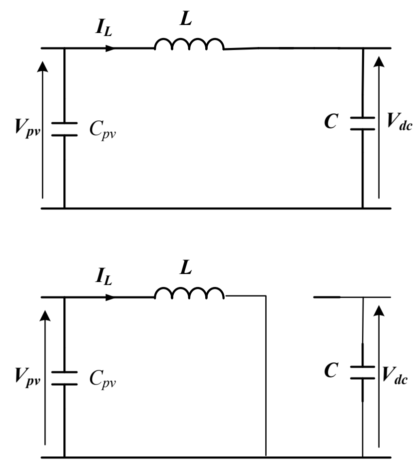

Figure 3. The DC/DC equivalent circuit.

The characteristic equations of this PV converter can be written as follows:

$$\frac{dI_{pv}}{dt} = \frac{V_{PV}}{L} \tag{5}$$

$$\frac{dI_{pv}}{dt} = \frac{V_{PV} - V_{dc}}{L} \tag{6}$$

where, V_{dc} and I_L are, respectively, the DC-link voltage and the boost inductance current.

Figure 4 shows the adopted MPPT method that is based on model predictive control (MPC) due to its ability to improve the PV systems efficiency.

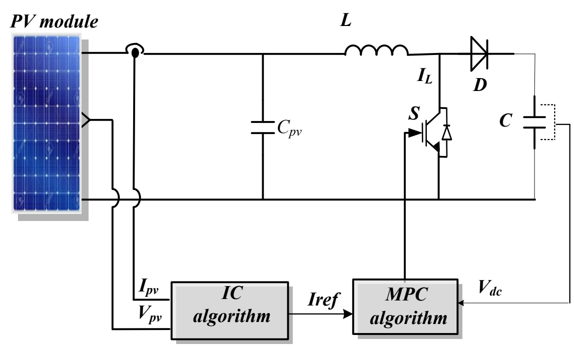

Figure 4. The photovoltaic converter block diagram.

Forward Euler method as expressed by (7) is utilized to get a discrete-time condition for the future anticipated PV current at inspecting moment (k + 1) as shown in (8) and (9):

$$\dot{x} \approx \frac{x(k+1) - x(k)}{T_s} \tag{7}$$

k is the current specimen instant and T_s is the sampling time

$$I_{pv(s=1)}(k+1) = I_{pv}(k) + \frac{Ts}{L}\left(V_{pv} - V_{dc}\right) \tag{8}$$

$$I_{pv(s=0)}(k+1) = I_{pv}(k) + \frac{Ts}{L}V_{pv} \tag{9}$$

As illustrated in Figure 5, the Incremental Conductance (IC) MPPT algorithm is applied to determine the PV reference current I_{ref} for the MPC. This considered technique aims to forecast the error between the current sampling time and its reference based on the cost function minimization. Thus, g^0 and g^1 cost functions are the significant key parameters of the MPC calculation; they will be determined for both exchanging states and decide for the one that guarantees the closest future anticipated an incentive to the reference current direction.

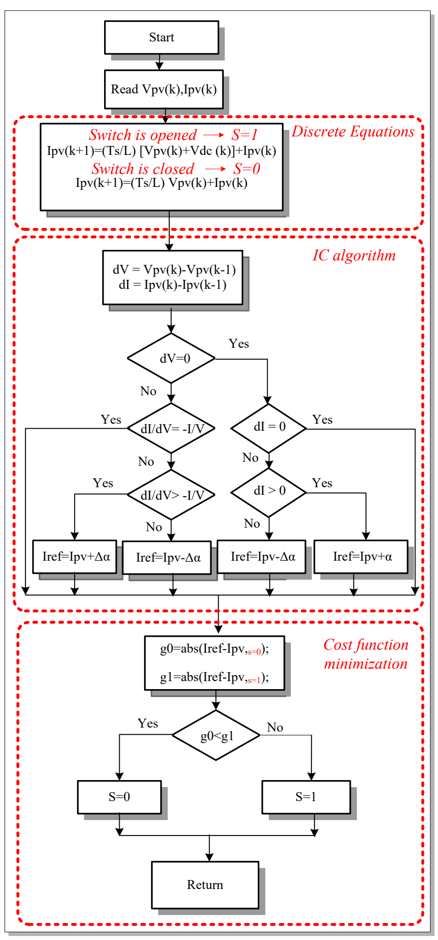

Figure 5. IC-MPC Flowchart.

4. Grid Connected PV Inverter Control

The control system of a grid-connected photovoltaic inverter is habitually divided into three parts. The first part aims to regulate the DC-link voltage based on an external control loop using a PI controller. Whereas an internal loop controls the d-q grid current components employed in the second part. Finally, the grid synchronization based on the usage of Stage Locked Loop (PLL) is applied in the last part to calculate the grid voltage position.

4.1 DC-link Voltage Control

To control the external loop, the DC-link voltage reference (V_{dc_ref}) is compared with DC voltage (V_{dc}) and the error signal is fed to a PI controller (with proportional gain $G_{i(dc)}$ and integral time constant $(\tau_{i(dc)})$ that is included to maintain the DC bus voltage constant as illustrated in Figure 6.

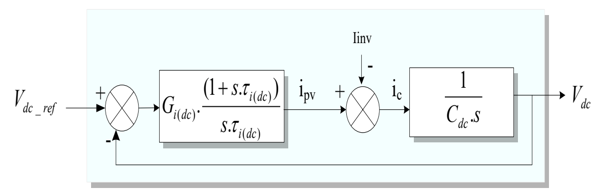

Figure 6. DC_link voltage loop.

By neglecting I_{inv} current effect, the closed-loop transfer function is given by the following relation:

$$FTBF_{dc}(s) = \frac{V_{dc}}{V_{dc\_ref}} = \frac{(1+s.\tau_{i(dc)})}{\frac{\tau_{i(dc)}.C_{dc}}{G_{i(dc)}}.s^2 + \tau_{i(dc)}.s + 1} \tag{10}$$

We can deduce the PI controller parameters by choosing the desired damping ratio $\zeta_{(dc)}$ and the natural oscillation frequency $\omega_{n(dc)}$.

$$G_{i(dc)} = 2.\zeta_{(dc)}.C.\omega_{n(dc)}) \tag{11}$$

$$\tau_{i(dc)} = \frac{2.\zeta_{(dc)}}{\omega_{n(dc)}} \tag{12}$$

4.2 The Grid Current Control

4.2.1 VOC Method for PV Inverter

The Grid Connected PV inverter schematic used the Voltage Oriented Control VOC is described by Figure 7. Typically, this method is based on the Park transformation of the i(a,b,c) grid currents wave forms to control the active and reactive power indirectly by their corresponding q current mechanisms. The classical controller's *PI* regulators are adopted in order to control the dqgrid currents where the direct grid current reference i_{gd_ref} is derived from the DC-link voltage loop, however, the quadrature grid current reference i_{gq_ref} is set to zero to obtain the unity power factor process.

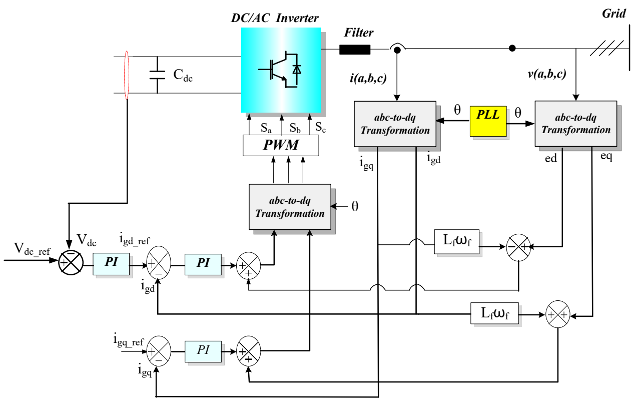

Figure 7. VOC for Grid connected inverter.

The obtained closed-loop transfer function has a form of a first order system with a time constants $\tau_{f(gd)} = \frac{L_f}{G_{i(gd)}}$ and $\tau_{f(sq)} = \frac{L_f}{G_{i(gq)}}$ where, $G_{i(gd)}$ is the proportional gain and L_f is the filter inductance.

$$FTBF_{gd}\left(s\right) = \frac{i_{gd}}{i_{gd\_ref}} = \frac{\frac{G_{i(gd)}}{s.L_f}}{1+\frac{G_{i(gd)}}{s.L_f}} = \frac{1}{1+\tau_{f(gd)}.s} \tag{13}$$

$$FTBF_{gq}\left(s\right) = \frac{i_{gq}}{i_{gq\_ref}} = \frac{\frac{G_{i(gq)}}{s.L_f}}{1+\frac{G_{i(gq)}}{s.L_f}} = \frac{1}{1+\tau_{f(gq)}.s} \tag{14}$$

The PI regulator parameters are calculated by choosing the time constant $t_{r(gd)}$ value (respectively $t_{r(gq)}$)

$$\begin{cases} G_{i(gd)} = 3.\frac{L_f}{t_{r(gd)}} \\ \tau_{f(gd)} = \frac{L_f}{G_{i(gd)}} \end{cases} \text{and} \begin{cases} G_{i(gq)} = 3.\frac{L_f}{t_{r(gq)}} \\ \tau_{f(gq)} = \frac{L_f}{G_{i(gq)}} \end{cases} \tag{15}$$

4.2.2 SMC Method for PV Inverter

The sliding mode theory was commonly employed for the grid connected converter due to its robustness against parameters variations as given by Figure 8, it is essentially divided into three steps. The appropriate sliding mode surfaces selection is achieved in the first step. The general equation used to choose these sliding surfaces is expressed by[15]:

$$S\left(X\right) = \left(\frac{d}{dt}+\lambda\right)^{r-1}\left(X^d - X\right) \tag{16}$$

where, X is the state variable of the control signal; λ is the positive constant, r is the system degree and X^d is the desired signal.

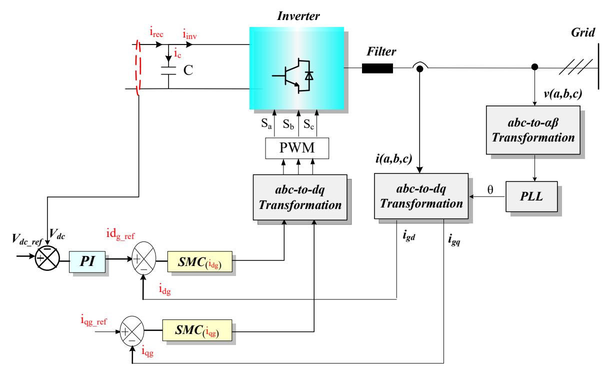

Figure 8. Sliding mode control for grid connected inverter.

In order to guarantee the convergence towards the sliding surface trajectory; the convergence condition based on Lyapunov equation is defined in the second step.

$$S\left(X\right)S\left(\dot{X}\right) < 0 \tag{17}$$

Finally, the control signal calculation is written by the following relation:

$$U = U_{eq} + U_n \tag{18}$$

where, U_{eq} is the equivalent control and U_n is the switching controls term.

Two switching surfaces are chosen $S\left(i_{dg}\right)$ and $S\left(i_{qg}\right)$ in order to regulate d-axis and q-axis grid current components.

$$\begin{cases} S\left(i_{dg}\right) = i_{dg\_ref} - i_{dg} \\ S\left(i_{qg}\right) = i_{qg\_ref} - i_{qg} \end{cases} \tag{19}$$

where, i_{dgf} , i_{qg} are the desired current values of d and q axis; The current references i_{dg_ref} and $i_{qg_{ref}}$ are maintained constants. Therefore, the sliding surfaces derivatives can be written as follows:

$$\begin{cases} \dot{S}\left(i_{dg}\right) = \dot{i}_{dg_{ref}} - \dot{i}_{dg} = -\dot{i}_{dg} = \dfrac{1}{L_f}\left(v_{dg} + R_f i_{dg} - \omega_f L_f i_{qg} - e_{dg}\right) \\ \dot{S}\left(i_{qg}\right) = \dot{i}_{qg_{ref}} - \dot{i}_{qg} = -\dot{i}_{qg} = \dfrac{1}{L_f}\left(R_f i_{qg} + \omega_f L_f i_{dg} - e_{qg}\right) \end{cases} \tag{20}$$

The sliding surfaces and their derivatives should validate the following conditions:

$$S\left(i_{dg}\right)\dot{S}\left(i_{dg}\right) < 0 \tag{21}$$

$$S\left(i_{qg}\right)\dot{S}\left(i_{qg}\right) < 0 \tag{22}$$

Therefore, the d-axis controlled voltage is defined by:

$$v_{dg\_ref} = v_{dg\_eq} + v_{dg\_n} \tag{23}$$

With

$$\begin{cases} v_{dg\_eq} = v_{dg} + R_f i_{dg} - \omega_f L_f i_{qg} \\ v_{dg\_n} = k_{dg}\, sgnS\left(i_{dg}\right); k_{dg} > 0 \end{cases} \tag{24}$$

The q-axis controlled voltage is defined by

$$v_{qg\_ref} = v_{qg\_eq} + v_{qg\_n} \tag{25}$$

With

$$\begin{cases} v_{qg_{eq}} = R_f i_{qg} + \omega_f L_f i_{dg} \\ v_{qg\_n} = k_{qg}\, sgnS\left(i_{qg}\right); q > 0 \end{cases} \tag{26}$$

5. The Proposed MPC Method for PV Inverter

The MPC algorithm is based on the mathematical model of three-phase inverter to predict the future grid current behavior for each seven voltage vectors (Table 1) distributed by the grid converter with two combinations $(V_0 = V_7)$ that produce zero voltage vector. So as to limit a predefined cost work that characterize a diminished blunder between the anticipated framework flows and their references, MPC-based calculation grant to choose and apply an ideal voltage vector.

Table 1. Converter voltage vectors

Switching states	S_{sa}	S_{sb}	S_{sc}	*Voltage vector*
1	0	0	0	V_0
2	1	0	0	V_1
3	1	1	0	V_2
4	0	1	0	V_3
5	0	1	1	V_4
6	0	0	1	V_5
7	1	0	1	V_6
8	1	1	1	V_7

As shown in the Figure 9, the output inverter voltage vectors $v_{c\alpha}(k)$ and $v_{c\beta}(k)$ are determined in stationary $(\alpha\beta)$ reference outline. They are reliant on the dc-connect voltage V_{dc} and the converter switching signals $S_a(k), S_b(k)$ and $S_c(k)$.

$$\begin{bmatrix} v_{c\alpha}(k) \\ v_{c\beta}(k) \end{bmatrix} = \frac{2}{3} V_{dc} \begin{bmatrix} 1 & -\frac{1}{2} & -\frac{1}{2} \\ 0 & \frac{\sqrt{3}}{2} & -\frac{\sqrt{3}}{2} \end{bmatrix} \begin{bmatrix} S_a(k) \\ S_b(k) \\ S_c(k) \end{bmatrix} \tag{27}$$

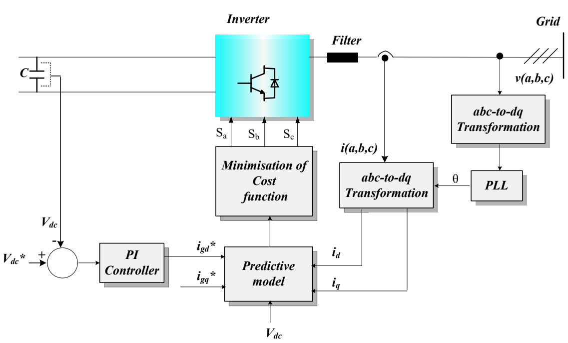

Figure 9. MPC-based algorithm for grid connected inverter.

The yield converter voltage vectors $v_{cd}(k)$ and $v_{cq}(k)$ are stated in dq reference frame:

$$\begin{bmatrix} v_{cd}(k) \\ v_{cq}(k) \end{bmatrix} = \begin{bmatrix} cos\theta(k) & sin\theta(k) \\ -sin\theta(k) & cos\theta(k) \end{bmatrix} \begin{bmatrix} v_{c\alpha}(k) \\ v_{c\beta}(k) \end{bmatrix} \tag{28}$$

Equations (29) and (30) can be expressed as follows in order to describe the predictive current controller algorithm:

$$\frac{di_{gd}}{dt} = \frac{v_{gd}}{L_f} - R_s \frac{i_{gd}}{L_f} - \frac{v_{cd}}{L_f} \tag{29}$$

$$\frac{di_{gq}}{dt} = \frac{v_{gq}}{L_f} - R_s \frac{i_{gq}}{L_f} - \frac{v_{cq}}{L_f} \tag{30}$$

The obtained system equations discretization for the predicted grid currents at sampling instant (k + 1) for each switching possibility as shown in (31) and (32):

$$i_{gd}^{p}(k+1) = \left(1 - T_s \frac{R_f}{L_f}\right) i_{gd}(k) + \frac{T_s}{L_f}[v_{gd}(k) - v_{cd}(k)] \tag{31}$$

$$i_{gq}^{p}(k+1) = \left(1 - T_s \frac{R_f}{L_f}\right) i_{gq}(k) + \frac{T_s}{L_f}[v_{gq}(k) - v_{cq}(k)] \tag{32}$$

where, R_f is the filter resistance and L_f is the filter inductance.

The cost capacity g is the blunder between the future anticipated current worth and its reference as written in condition (27), it will be determined for every one of the seven conceivable voltage vectors created by the three stages inverter and pick the one with the anticipated current worth closer to the ideal worth.

$$g = \left|i_{ref} - i_{gd}^{p}(k+1)\right| + \left|i_{ref} - i_{gq}^{p}(k+1)\right| \tag{33}$$

6. Grid Synchronization

The renewable energy sources output has generally a random behaviour due of the random variations in weather conditions. So, to achieve a precise synchronization between the photovoltaic energy source and the grid, a Phase Locked Loop (PLL) is required in order to compute the grid voltage position theta. A PI controller is applied to reduce to zero the difference between the grid phase angle and the inverter phase angle as shown in Figure 10. Psim environment is utilized for the re-enactment of single stage inverter to synchronize it with the framework, as far as voltage, recurrence and stage.

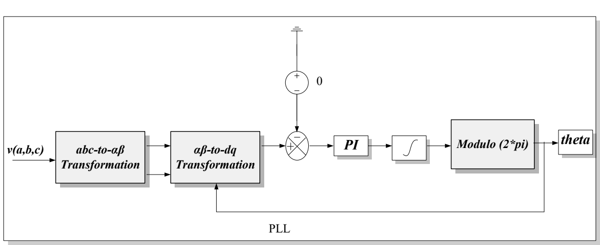

Figure10. Structure of a single phase PLL.

7. Results and Discussion

As a perspective to validate the photovoltaic system model and prove the proposed MPC algorithm effectiveness, simulation examinations are built on PSIM Software considering the specification system parameters given in Table 2.

Table 2. Photovoltaic panel parameters

PARAMETER	Value
Maximum Power Point	200 W
Maximum Power Point Voltage	26.3 V
Maximum Power Point Current	7.61 A
Open Circuit Voltage	32.9 V
Short Circuit Current	8.21 A

Simulation results and energy performance analysis of 7.5 kW grid-connected PV system are based on irradiation condition levels as shown in Figure 11 (a). At t = 0.5s, solar irradiance is increased from 700 to 1000 W/m^2 and decreased from 1000 W/m^2 to 400 W/m^2 at t = 1s. The photovoltaic system with twelve panels in series and three arrangements working in parallel at constant temperature T at 25°C.

It can be seen in Figure 11 (b) that the produced power Ppv utilizing a prescient controller pursues the reference control Pmax with great precision.

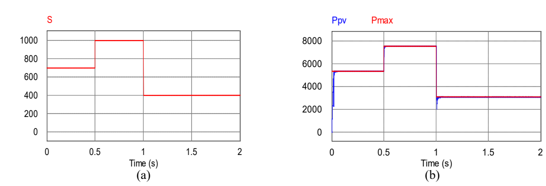

Figure 11. (a) Solar irradiance levels, (b) Ppv output power and its Pmax reference.

The Figures 12 (a) and (b) showed respectively the maximum output current I_{pv} and the maximum output voltage at the boost converter output which are highly reliant on climatic circumstances to have a good track to the optimal power value.

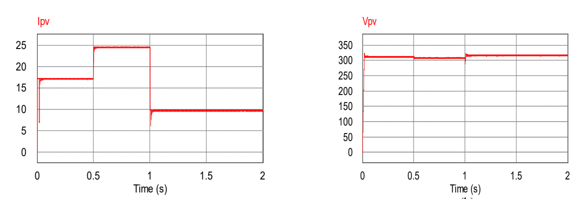

Figure 12. (a) PV generator current, (b) PV generator voltage.

Figures 13 and 14 show the simulation tests of grid connected photovoltaic inverter using the VOC method. It can be noted in Figure 13 that the injected grid currents have a sinusoidal waveforms with a continuous grid frequency value equal to 50 Hz, however, a large overshoot occurs during a climatic condition changes and the obtained grid current THD is equal to 5.6%. Overshoots are seen also in the active power signal as shown in Figure 14.

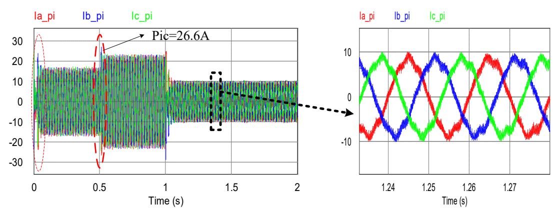

Figure 13. Grid currents waveforms using VOC.

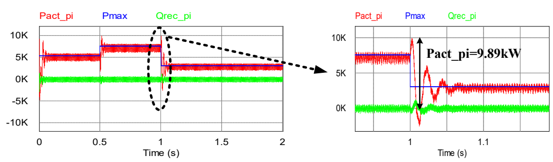

Figure 14. Active and reactive power using VOC.

The simulation results of the SMC strategy are illustrated respectively in Figures 15 and 16. It can be seen in Figure 15 that the grid currents contain several harmonics which is lead to generate a larger current THD 7.8%. The active and reactive power depicted in Figure 16, follow the desired powers but they have a high harmonic distortion.

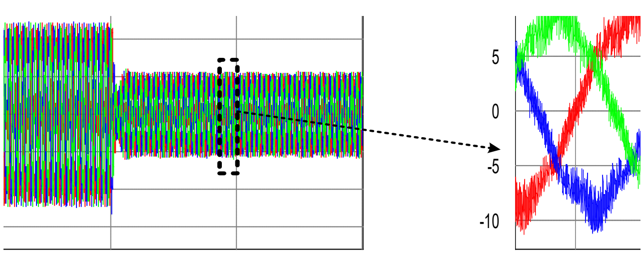

Figure 15. Grid currents waveforms using SMC.

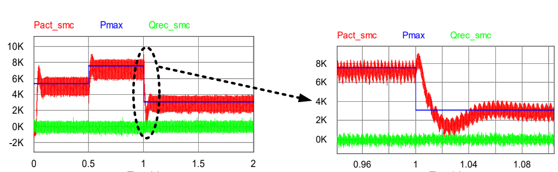

Figure 16. Active and reactive power using SMC.

Simulation results conducted to verify the proposed MPC-algorithm performances are shown in the graphs below. It can be noticed in Figure 17 that the sinusoidal grid currents wave forms dependent on weather conditions, increase and decrease when solar irradiance changes. The current quality is evaluated by calculating the current THD value which is equal to 3.7%. Figure 18 illustrates respectively the injected active and reactive power into the grid. It is clear that the improved active power signal follows perfectly its reference power (Pmax) according to solar irradiance. The reactive power injected to the grid is set at zero in order to achieve the unity power factor condition.

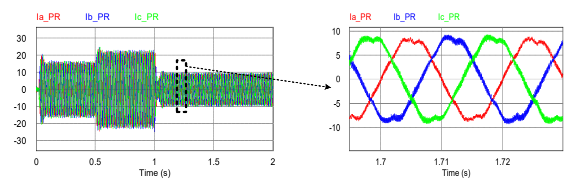

Figure 17. Grid currents waveforms using MPC.

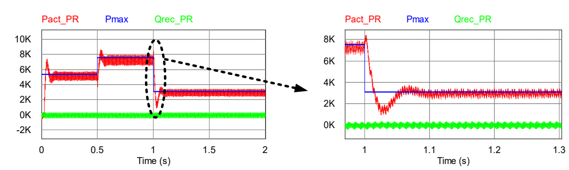

Figure 18. Active and reactive power using MPC.

The DC-link voltage is maintained constant over the time period of 2 secs as shown in Figure 19; it follows correctly its reference value Vdc_ref = 750V. It can be observed that the DC voltage over shoots are significantly small due to the climatic condition variations. The synchronization signal is shown in Figure 20.

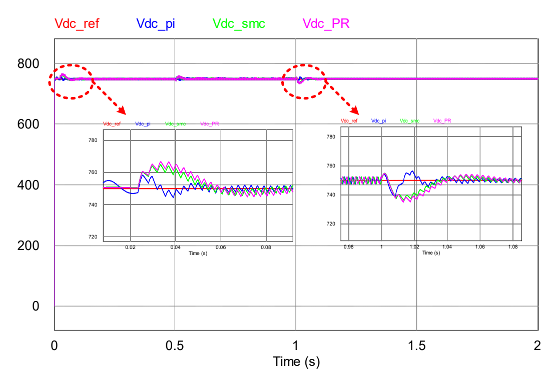

Figure 19. DC link voltage control.

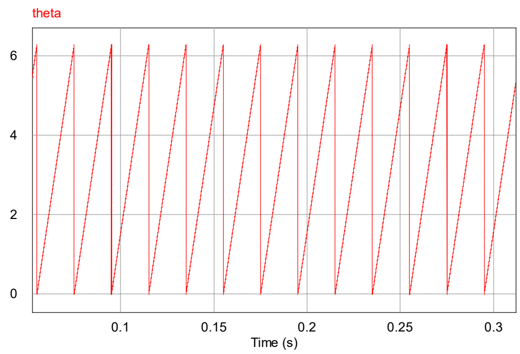

Figure 20. Grid voltage position.

8. Comparative Study

For a good evaluation of the proposed MPC-algorithm applied for a grid connected inverter, a comparison of its performances with others VOC and SMC conventional methods is required. Several key criteria for the comparison between these control schemes are considered such as the current THD, the overshoots, the switching frequency, the power distortion and the robustness against parameter variations.

The simulation tests show that the MPC technique offers a minimum grid current THD 3.7% compared to the two others standard strategies. It is remarkable also how the overshoots appear in the current and power curves due the sudden variation of meteorological conditions, the control scheme using VOC algorithm provide a larger undesirable overshoot rates than SMC and MPC behaviors as shown in Figure 13 and Figure 14. The active and reactive power distortion generated by the proposed MPC-algorithm is lower compared to the linear controller and sliding mode controller (Figure 18). It can be deduced that the VOC method present a fixe switching frequency, besides, in the case of the SMC and model predictive control the switching frequency is variable depending on the operating point.

9. Conclusion

In this work, comparative investigation between the VOC linear controller, the non-linear SMC technique and the Model Predictive Control (MPC) is presented to control the grid connected photovoltaic inverter. Compared to the classical VOC and sliding mode control, the proposed MPC algorithm offered lower grid currents THD and allowed a minimum active and reactive power distortion. The obtained Psim simulations validate the effectiveness of the proposed MPC method against parameter variations. As a future step, an implementation of these different algorithms will be designed. An experimental testing platform is intended by using the STM32F4 microcontroller as a digital target support, the SEMITEACH-IGBT as a power inverter and the measurement board which used to give current and voltage measures. The experimental techniques comparison will be discussed and their performance parameters will be tested and evaluated.

10. Acknowledgement

This work was upheld by the Tunisian Ministry of High Education and Research under the course of LAPER lab.

11. References

1. Bounechba H, Bouzid A, Nabti K, Benalla H. Comparison of perturbs and observe and fuzzy logic in maximum power point tracker for PV systems. Energy Procedia. 2014; 50:677–84. https://doi.org/10.1016/j.egypro.2014.06.083.
2. Tasooji TK, Mostafazadeh A, Usta O. Model predictive controller as a robust algorithm for maximum power point tracking. 10th International Conference on Electrical and Electronics Engineering (ELECO); 2017. p. 1–12.
3. Abdel-Rahim O, Funato H. Model predictive control based maximum powerpoint tracking technique applied to ultra step-upboost converter for PV applications. 2014 IEEE Innovative Smart Grid Technologies - Asia (ISGT ASIA); 2014. p. 1–10 https://doi.org/10.1109/ISGT-Asia.2014.6873778. PMid:24572456
4. Model predictive control for PV maximum powerpoint tracking of single-phase sub multilevel inverter [Internet]. [cited 2016 Feb]. Available from: https://www.researchgate.net/publication/292986327_Model_Predictive_Control_for_Maximum_Power_Point_Tracking_of_Single-Phase_SubMultilevel_Inverter_for_Photovoltaic_Systems.
5. Karamanakos P, Geyer T, Manias S. Direct voltage control of DC-DC boost converters using enumeration-based model predictive control. IEEE Transactions on Power Electronics. 2014; 29(2):968–78. https://doi.org/10.1109/TPEL.2013.2256370.
6. Abdel-Rahim O, Funato H, Haruna J. An efficient MPPT technique with fixed frequency finite-set model predictive control. Energy Conversion Congress and Exposition (ECCE); 2015. p. 1–6. https://doi.org/10.1109/ECCE.2015.7310562.

7. Rao MV, Reddy MP, Reddy BS. Voltage oriented control of a grid connected PV system by modified MPPT algorithm. International Journal of Professional Engineering. 2013; 1(2):72–82.
8. Direct power control of a grid connected photovoltaic system, associated with an active power filter [Internet]. [cited 2018]. Available from: https://www.springerprofessional.de/en/fuzzy-direct-power-control-of-a-grid-connected-photovoltaic-syst/15527846.
9. Sliding mode control strategy for grid connected PV system [Internet]. [cited 2017]. Available from: https://www.semanticscholar.org/paper/Sliding-mode-control-strategy-for-grid-connected-PV-Youssef-Sbita/211b56ae8b5c6804d6b827182d933414d88378ef.
10. Kalyanraj D, Prakash SL, Arutchelvi M. Design of sliding mode controller for three phase grid connected photovoltaic system. International Journal of Control Theory and Applications. 2015; 8(3):1097–103.
11. Hassine, IM-B, Naouar MW, Mrabet-Bellaaj N. Model based predictive control for three-phase grid connected converter. Journal of Electrical Systems. 2015; 11–4:463–75.
12. Ahmadi A, Ahmadifar MJ, Ahmadi S. Three-phase inverter control by model predictive control. Research Journal of Recent Sciences. 2015; 4(1):81–6.
13. Rohten JA, Espinoza JR, Munoz JA, Pérez MA, Melin PE, Silva JJ, Espinosa EE, Rivera ME. Model predictive control for power converters in a distorted three-phase power supply. IEEE Transactions on Industrial Electronics. 2016; 63(9):5838–48. https://doi.org/10.1109/TIE.2016.2527732.
14. Song Z, Tian Y, Chen Z, Hu Y. Enhanced predictive current control of three-phase grid-tied reversible converters with improved switching patterns. Energies. 2016; 9(1):1–16. https://doi.org/10.3390/en9010041.
15. Nasiri M, Milimonfared J, Fathi SH. Robust control of PMSG-based wind turbine under grid fault conditions. Indian Journal of Science and Technology. 2015; 8(13):1–13. https://doi.org/10.17485/ijst/2015/v8i13/52201.